

CORROSION BEHAVIOR OF DOUBLE-GLOW PLASMA COPPERIZING COATING ON Q235 STEEL

Z.-G. Yang ^{a,*}, W.-P. Liang ^{a,*}, Y.-L. Jia ^{b,c,*}, Q. Miao ^a, Z. Ding ^a, Y. Qi ^a

^a School of Materials Science and Technology, Nanjing University of Aeronautics and Astronautics, Nanjing, China

^b College of Materials Science and Engineering, Central South University, Changsha, China

^c College of Materials Science and Technology, Beijing University of Technology /100 Ping Le Yuan, Chaoyang District, Beijing, China

(Received 20 August 2019; accepted 25 June 2020)

Abstract

In this paper, the copperized layer was fabricated on the surface of Q235 steel via double glow plasma surface alloying technology to improve the marine fouling organisms attached on the surface of marine structures. The microstructure and phases composition of the coating were analyzed by SEM and XRD. The corrosion characteristics of substrate and coating were investigated in 3.5wt.% NaCl solution. The results indicated that the protective coating had a novel structure of an outermost deposition layer (85 μm) and inner diffusion layer (51 μm), which exhibited great adhesion stress because of the metallurgical bonding effects. The corrosion characteristics of substrate and coating were analyzed in detail. The corrosion products of Q235 steel were mainly β-FeOOH, γ-FeOOH, and α-FeOOH in the early stage of corrosion process. Then the whisker-like structure of α-FeOOH grew on the surface of γ-FeOOH and the β-FeOOH transformed into γ-FeOOH to achieve thermodynamical equilibrium. The dissolved copper ions in solution resulted in a unique difference in the formation of corrosion products, which inhibited the transition of iron hydroxide and promoted the formation of amorphous phases. Based on electrochemical measurement, the coating had lower corrosion current density and higher charge transfer resistance than substrate. The corrosion resistance of copperized layer was better than that of Q235 steel.

Keywords: Double glow plasma technology; Plasma surface metallurgy; Copperized layer; Antifouling coatings; Corrosion characteristics; Rust layer

1. Introduction

The attachment of marine fouling organisms (the general name of animals, plants, and microbial species) on offshore installations or ships could cause irretrievable destruction and economic loss. Marine fouling organisms attach and multiply on the surface of marine structures, which could cause adverse effects and even destroy the attached materials in final. Generally, the formation of marine fouling community can be divided into a four-step process: Primary film formation, Biofilm formation, Diatom and protozoan colonization, and Settlement of invertebrate larvae and algal spores [1, 2]. The so-called antifouling is inhibiting the colonization of algal cells during the second and third stages, which further interrupts the settlement of larger marine invertebrates or other large organisms.

Therefore, many methods are carried out to prevent the attachment of marine fouling organisms.

The most antifouling methods usually originate from the release of biocides (Cu, Sn). Preparing antifouling coating is commonly employed means due to its advantages of simplicity, convenience, and high efficiency. Chang L et al. [3] pointed out that tributyltin self-polishing copolymer paint (added with organotin compounds) possesses good antifouling ability on the basis of copper compounds (Cu₂O, CuSCN). However, the paint contains metallic oxide or organics which cause a serious pollution to the ocean [4, 5]. Xiang Gao et al. [6] reported that the 316L stainless steel was electroplated with copper, which improved the corrosion resistance. Nevertheless, those methods (painting and electroplate) had a serious flaw that was the poor adhesion between the coating and substrate. Thus, looking for a novel method to fabricate coatings is necessary.

In recent years, double glow plasma surface alloying technology (DG Technique) is used as a

*Corresponding author: wpliang@nuaa.edu.cn; 438099980@qq.com; jiayanlin@126.com



novel method in surface modification, which is considered as a new kind of physical vapor deposition technology. DG technique has been employed successfully to fabricate many coatings, such as Ni, Zr, and Mo, etc [7-10]. DG technique employs the plasma region produced by double glow discharges is the most remarkable characteristic. The target stroked by Ar^+ with high ionization and the beneficial elements is sputtered to diffuse into the substrate. The coating fabricated by double glow process has the gradient structure, and the adhesion stress between coating and substrate is great because of the metallurgical bonding effects [11]. In addition, the application of DG technique can save precious metal resources and reduce energy consumption.

In this paper, the copperized layer was fabricated on Q235 steel via double glow plasma surface alloying technology. The microstructure and phase constituents of copperized layer were determined, and corrosion behaviors of coating and substrate in 3.5% NaCl solution were investigated. The corrosion mechanism at different immersion time was discussed.

2. Experiment

The samples of Q235 steel was a kind of low carbon steel, and the chemical composition (wt.%) of Q235 steel was 0.35 Mn, 0.3 Si, 0.18 C, ≤ 0.04 S, ≤ 0.04 P, and the rest of it was Fe. The samples were cut into 15 mm \times 15 mm \times 4 mm pieces by wire cutting. All samples were polished by water proof abrasive paper of 1000 meshes, then cleaned in ethanol to remove contamination.

Fig.1 shows the sketch of double glow plasma surface alloying machine. The target was mounted on the source electrode and the position of cathode was matrix. Argon was used as background gas, which was stimulated as active argon ions because of the double glow discharge. The target and sample were covered by glow discharge, which transferred heat

and ions during the sputtering process from target to sample due to the active ions (Ar^+) that hit the target incessantly. Furthermore, bombardment of argon ions can also activate the substrate-surface which promoted the diffusion of beneficial elements. In this study, copperized layer was manufactured by DG treatment. Pure copper (99.99%) target with size of $\Phi 120$ mm \times 4 mm was used as source electrode material. The experimental parameters are listed in Table 1.

The surface and cross-sectional morphologies of copperized layer were examined by emission scanning electron microscopy (SEM, Hitachi S-4800). The phase compositions of the coating were analyzed by X-ray diffraction (XRD, BrukerD8-ADVANCE) with copper $K\alpha$ radiation ($\lambda = 1.5418$ Å).

Furthermore, the open-circuit potential measurements (E_{corr}), potentiodynamic polarization curves and electrochemical impedance spectroscopy (EIS) were carried out to evaluate the corrosion resistance of copperized layer using CHI660D electrochemical workstation with a three-electrode cell system in stationary 3.5 wt.% NaCl solution. The working electrode was the sample, which was sealed by epoxy resin with a surface area of 1.0 cm^2 exposed. The platinum electrode was used as auxiliary electrode with 4.0 cm^2 surface exposed, and the saturated calomel electrode (SCE) was used as reference electrode. The EIS spectra was detected according to open-circuit potential (E_{corr}) with scanning range from 1 MHz to 0.01 Hz. The potentiodynamic polarization test was carried out in a range of ± 0.5 V of open circuit potential. Results were analyzed, and the equivalent circuits were fitted by ZSimpWin software. The Chi-square value (χ^2) of fitted equivalent circuit was less than $5\text{E}-04$, which ensures the fitting error of each equivalent element lower than 5%.

Table 1. The experimental parameters of the double glow plasma alloying

Parameter	Values
The voltage of the source electrode (V)	950
The voltage of the cathode (V)	550
Working pressure (Pa)	35
Distance between the source electrode and cathode (mm)	15
Treatment time (h)	3
Argon flow rate (sccm)	70

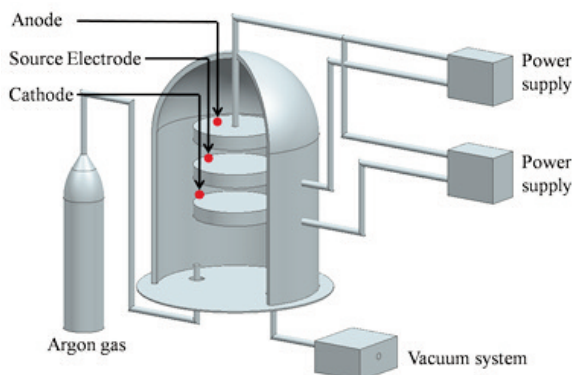


Figure 1. Sketch of Double Glow Plasma Surface Alloying Machine



3. Results and discussion

3.1. Microstructure of copperized layer

Fig. 2 reveals microstructure of copperized layer on Q235 steel. Cross-section morphology of copperized layer (Fig. 2a) indicates that the coating had no obvious defects, and it consisted of deposited layer and diffusion layer. Fig. 2c shows line scan result of copperized layer on Q235 steel, the result analyzed with Fig. 2a indicates that the thickness of copperized layer was 136 μm (85 μm deposition layer and 51 μm diffusion layer). The distribution of copper element was gradient at the interfaces due to the metallurgical bonding effects, which was a typical feature of double glow plasma alloying technology. During double glow treatment, the argon was stimulated as Ar^+ because of double glow discharged, the surfaces of target and substrate were activated due to the bombardment by Ar^+ with a certain high kinetic energy. The copper atoms were sputtered from target to substrate and diffused into the surface under the high temperature device chamber environment. The adhesion between coating and substrate was strong enough due to the metallurgical bonding effects [11]. During the DG process, cupric ions were sputtered from target and penetrated into the substrate because of the sufficient energy. Surface morphology of copperized layer (Fig. 2b) shows that uneven

columnar crystals of copper grew on the surface. Holes with 1-5 μm appeared on deposition layer uniformly due to the bombardment of argon ions or the columnar growth mechanism of copper. XRD pattern of copperized layer (Fig. 2d) shows that the main phase was Cu, and small amount of Fe existed in copperized layer.

3.2. Surface morphology and phases in corrosion products

The corrosion morphologies of Q235 steel in 3.5 wt.% NaCl solution at immersion times of 72 h, 360 h, and 672 h are shown in Fig. 3, respectively. Fig. 3 (a, c, and e) show the inner corrosion morphologies (removing unstable rusty layers) covered with black corrosion products. Fig. 3 (b, d, and f) show the outer corrosion product layer with the color of bright yellow. Fig. 3a shows inner corrosion morphology of Q235 steel at immersion times of 72 h. The results indicated that substrate was corroded uneven at the initial stage, the intergranular corrosion occurred firstly due to the disordered atomic arrangement and high internal stress at the grain boundary. Fig. 3 (c and e) show inner corrosion morphologies of Q235 steel at immersion times of 360 h and 672 h, respectively. The results suggest that lamellar structure appeared. The lamellar spacing was larger, which attribute to the

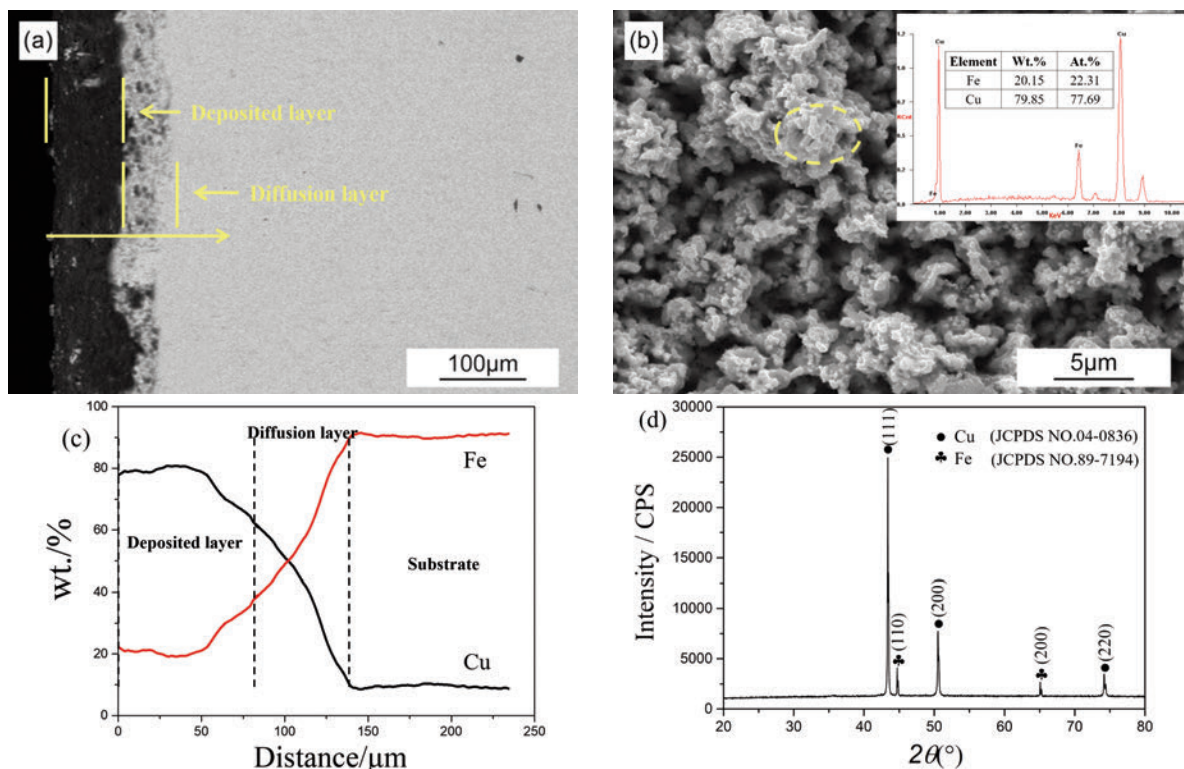


Figure 2. Cross-section morphology (a), surface morphology (b), EDS result (c) and XRD pattern (d) of prepared copperized layer

formation of micro-galvanic corrosion cells between the pearlite and ferrite. The ferrite was eroded preferentially as anode during the process of oxygen diffuse through outer rust layer.

Generally, typical corrosion products of carbon steel in NaCl solution mainly included needle-like or whisker-like goethite (α -FeOOH), large plate-like akaganeite (β -FeOOH), glomerate-like laminas of lepidocrocite (γ -FeOOH), and solid globular-like magnetite particles (Fe_3O_4) [12, 13]. As shown in Fig. 3b, main phase of corrosion products was β -FeOOH, and small amount of γ -FeOOH were observed. In addition, small amount of α -FeOOH which grew on the surface of γ -FeOOH could be found clearly. With the extension of corrosion time (Fig. 3d and f), the

main corrosion products transformed to γ -FeOOH, α -FeOOH, and Fe_3O_4 . The whisker-like structure of α -FeOOH grew on the surface of γ -FeOOH, which was observed more clearly. Many scholars pointed that [14-16] the initial corrosion product was γ -FeOOH during the corrosion process of carbon steel, the particles of α -FeOOH nucleated and grew on the surface of γ -FeOOH gradually with corrosion process progression. Meanwhile, β -FeOOH also transformed into γ -FeOOH due to the thermodynamically equilibrium [17].

Fig. 4 shows the corrosion morphologies of the coating at immersion times of 72 h, 240 h, 504 h, and 672 h, respectively. As shown in Fig. 4 (a and b), no obvious damage could be found on the coating and the

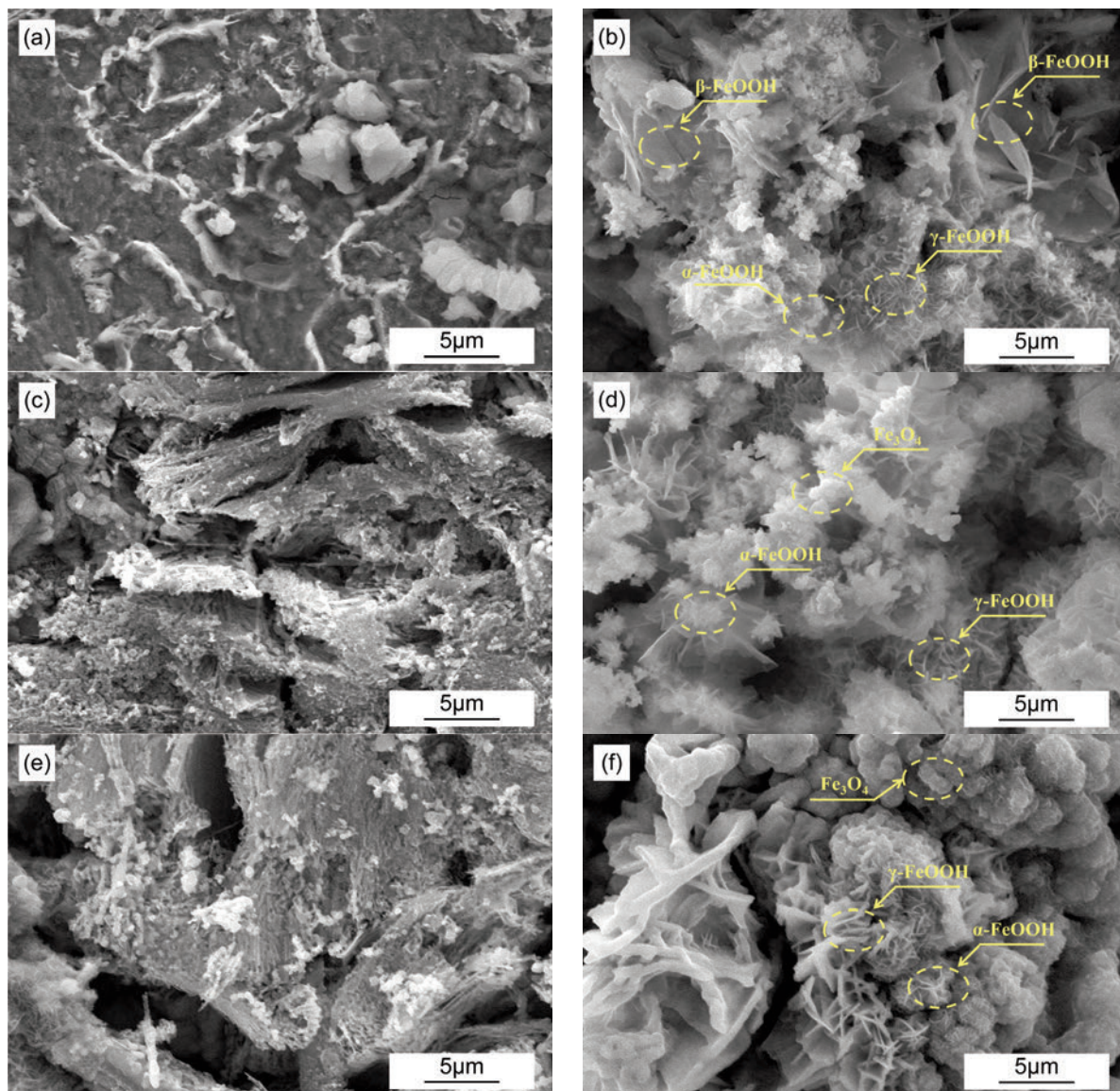


Figure 3. Typical corrosion morphologies of inner corrosion product layers ((a), (c), (e)) and outer corrosion product layer s((b), (d), (f)) formed on the surface of Q235 steel in 3.5 wt.% NaCl solution after the immersion for 72 h, 360 h, and 672 h, respectively

corrosion products formed on the surface became thicker and denser gradually. In the case of corrosion for 504 h (Fig. 4c), the coating was destroyed, the evident holes were observed on the surface. Corrosion products with different size grew on surface of copperized layer. With the extension of corrosion time, the formation of corrosion products led to uneven stress distribution. With the attack of chloride ions, the original corrosion products layer was desquamation, the coating was destroyed.

The EDS results of areas (area I to area VIII) marked in Fig. 4) of the coating after corrosion test are listed in Table 2. With the extension of corrosion time, the depth of the holes on coating was larger, and the integral morphology of coating was basically consistent. In particular, the content of oxygen was always less 4 wt.% even after 672 h immersion, and the content of Cu was seriously degraded with the extension of corrosion time. The results analyzed from Table 2 indicate that the oxidation of copperized layer was slight. In short, a large amount of copper dissolved into solution, which could improve the property of marine biofouling resistance.

In addition, the corrosion products were dominated by Fe element. During the corrosion process, NaCl solution passed through the holes and reacted with iron at the bottom of coating. Based on electrochemical reaction, iron was preferentially

dissolved to form Fe^{3+} , which was reduced by Cu to form Fe^{2+} , the Cu also turned into copper ions at the same time. The coating was destroyed seriously and even substrate was exposed due to the formed of corrosion products and the dissolution of Cu. Anyhow, corrosion products were mainly ruling by iron, and copper was mainly dissolved in the solution.

Furthermore, the morphologies of corrosion products were acicular or strip shaped at the initial stage (area II). With the extension of corrosion time, the morphologies of corrosion products were denser and surrounded by bright white central agglomeration

Table 2. The EDS results of the areas (area I to area VIII) of the copperized layer after corrosion test

	O	Cl	Fe	Cu
Area I, (wt.%)	1.7	0.25	7.2	90.85
Area II, (wt.%)	10.52	0.37	74.8	14.32
Area III, (wt.%)	0.93	0.2	20.9	77.97
Area IV, (wt.%)	8.32	0.85	69.14	21.69
Area V, (wt.%)	2.38	-	32.7	64.92
Area VI, (wt.%)	12.72	2.35	84.94	-
Area VII, (wt.%)	2.72	-	38.27	59.01
Area VIII, (wt.%)	3.59	-	96.41	-

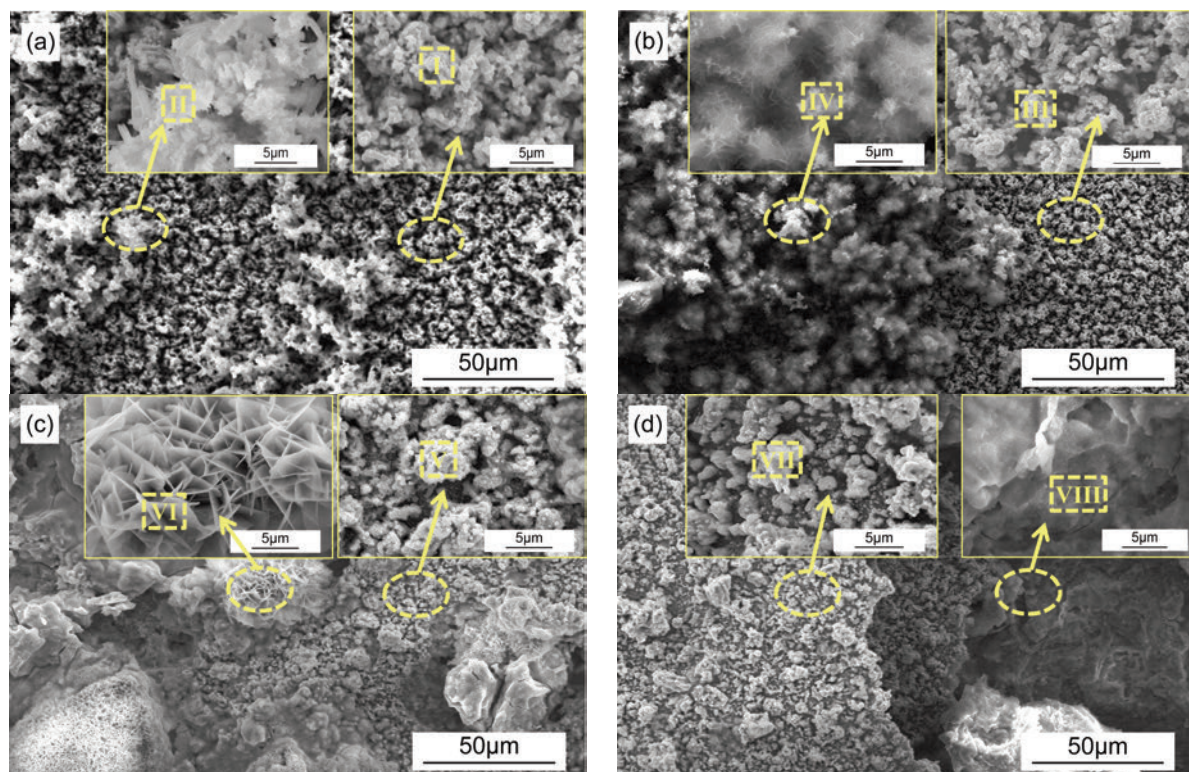


Figure 4. Typical corrosion morphologies formed on the surface of copperized layer in 3.5 wt.% NaCl solution after the immersion for 72 h, 240 h, 504 h and 672 h, respectively

and whisker (area IV). Corrosion products contained a small amount of copper due to the dissolution or adsorption of copper during corrosion process. Area VI in Fig. 4c shows the morphology of corrosion product after immersion for 504 h. γ -FeOOH appeared on the surface, which had a dense sheet structure. Many scholars pointed that [18-20] the formation of crystalline phases of iron were inhibited by copper ions. Fig. 4c shows the cylindrical amorphous phase grew vertically, and the morphology of amorphous phase was detected minutely in Fig. 4d (area VIII). The results indicate that peeling-off of the coating accelerated and even substrate was exposed because of the vertical growth of amorphous phase.

The corrosion products shown in Fig. 3 and Fig. 4 were verified by XRD technique (Fig. 5 and Fig.6). During the corrosion process of Q235 steel, the corrosion products were mainly β -FeOOH, γ -FeOOH, and α -FeOOH at initial stage. With the extension of immersion time, β -FeOOH disappeared, the α -FeOOH grew on the surface of γ -FeOOH. The Fe_3O_4 phase appeared and became the main component of the rust layer.

The XRD analysis of the coating is shown in Fig. 6. The intensity of diffraction peaks of Cu declined with the extension of corrosion time, which indicated the copper was corroded and dissolved gradually in the solution during corrosion process. Iron hydroxide was the primitive corrosion product of iron, which could transform into γ -FeOOH rapidly in some cases. As shown in Fig. 6, the transition of iron hydroxide was impeditive by copper ions. Many scholars pointed that [21, 22] the bonding of hydroxyl in oxyhydroxide could be destroyed by copper ions. The formation of oxide or oxyhydroxide of iron could be inhibited by copper ions. The raised curves shown in the low angle region of Fig. 6 indicated the formation of amorphous phases during the corrosion process, which became larger with the extension of corrosion time. The conclusion could be inferred that the

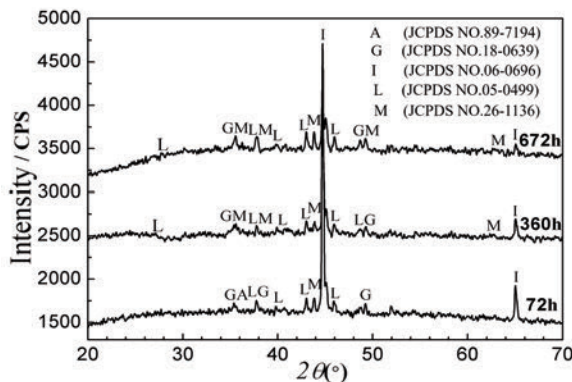


Figure 5. XRD pattern of Q235 steel at immersion times of 72 h, 360 h and 672 h, respectively. (A: β -FeOOH, G: α -FeOOH, I: Fe, L: γ -FeOOH, M: Fe_3O_4)

formation of corrosion products was affected by copper ions to depress the crystallinity of corrosion products and promote the amorphous phase.

3.3. Electrochemical characteristics

The variation in open-circuit potential with the extension of corrosion time usually reflects the transformation of electrochemical activity. Fig. 7 exhibits the variation of corrosion potentials of Q235 steel and copperized layer in 3.5 wt.% NaCl solution at different testing time. The corrosion potentials of substrate and coating shifted to more negative value rapidly at the corrosion time of 0 h-10 h. Then the corrosion potential of coating was stable at -0.72 V basically, while that of substrate was stable at -0.75 V initially and kept stable at -0.72 V after 450 h. Generally, the evolution of corrosion potential was closely related to the types of electrode materials and the ratio of electroactive areas [23, 24]. Therefore, it can be inferred that the corrosion reaction of substrate and coating was similar, which was mainly based on the anodic dissolution of iron. In addition, the copper

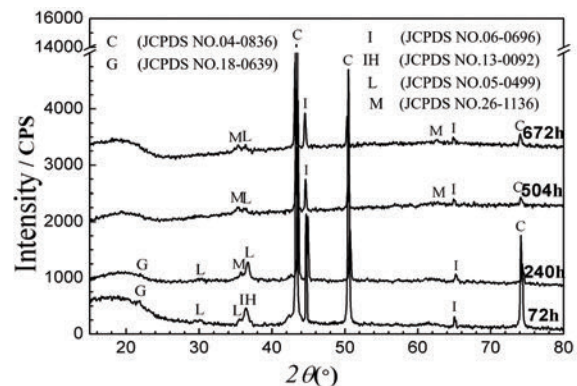


Figure 6. XRD pattern of copperized layer at immersion times of 72 h, 240 h, 504 h and 672 h, respectively. (C: copper rich phase, G: α -FeOOH, I: Fe, IH: iron hydroxide, L: γ -FeOOH, M: Fe_3O_4)

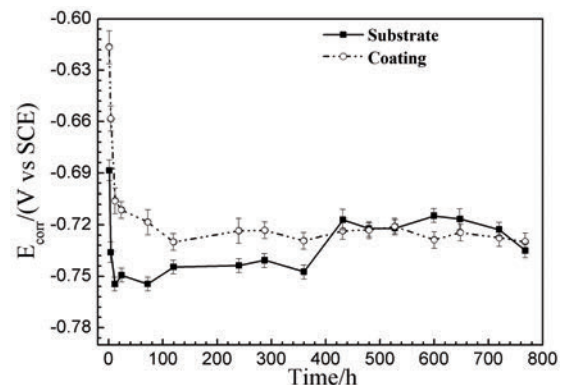


Figure 7. Evolution of corrosion potential with immersion time of Q235 steel and copperized layer in 3.5 wt.% NaCl solution



ions had a certain influence on the corrosion reaction, and corrosion resistance of the coating was slightly better than substrate before 450 h, which attributed to the grain refining effect of copper ions.

The potentiodynamic polarization curves of substrate and copperized layer are presented in Fig. 8 to evaluate the electrochemical characteristics. During the potentiodynamic polarization measurement, the variation of corrosion potentials of substrate and coating were inconspicuous. In spite of the observed passivation in anodic area of both samples, it could not improve the corrosion resistance due to the high passivity current density and narrow passivation range.

In addition, the corresponding corrosion current density i_{corr} ($\mu\text{A}/\text{cm}^2$), corrosion potential E_{corr} (V vs. SCE), cathodic Tafel slope β_c (mV/dec), and anodic Tafel slope β_a (mV/dec) are listed in Table 3. The corrosion current densities of the substrate were higher than that of coating, indicating that the coating could improve the corrosion resistance of steel. Furthermore, the corrosion current density of substrate and coating basically increased with the extension of time, indicating the accelerating corrosion rate during the immersion.

It should be noticed that the corrosion current densities of both lied in a relatively higher value at the

initial 24 h, which might attribute to the incomplete rust layer and the absorption of chloride ions. Subsequently, as the rust layer generated continuously with the increasing time, the adsorption of chloride ions was gradually inhibited, consequently the corrosion rate slowing down.

Besides, the anode slopes of substrate and coating were larger than the cathode slopes contemporaneously, which indicated that the corrosion reaction was controlled by anode reaction. Previous studies [25] suggested that the anode reaction was dominated by typical mass transfer control when the slope was over 60 mV/dec. Hence, it can be concluded that the anodic dissolution of iron and copper were the main potential determining reaction. The cathode slopes of coated samples were larger than substrate while the anode slopes showed an opposite trend, which indicates that the coating accelerated the anodic dissolution and inhibited the cathode reaction.

The impedance measurement is an effective method to evaluate the corrosion behavior of the interface between solution and metal. The Nyquist plots and Bode plots of substrate and the coating at different immersion time in 3.5 wt.% NaCl solution are shown in Fig. 9. The Nquist plots characterized a typical capacitive loops which indicated the charge

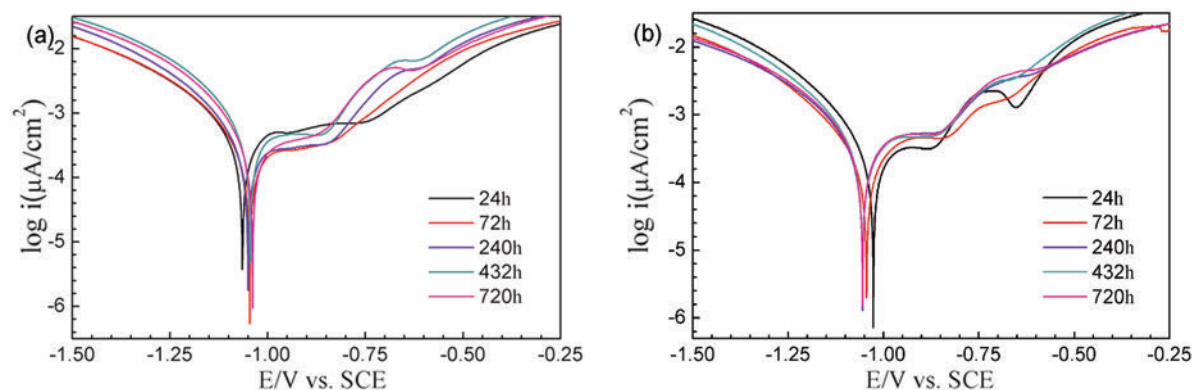


Figure 8. Potentiodynamic polarization curves of Q235 steel(a) and the copperized layer(b) at different times of immersion

Table 3. Electrochemical parameters evaluated from potentiodynamic polarization curves

specimen		I_{corr} ($\mu\text{A}\cdot\text{cm}^{-2}$)	E_{corr} (V vs.SCE)	β_c (mV/dec)	β_a (mV/dec)
Substrate	24 h	214.9	-1.065	82	161
	72 h	174.6	-1.046	95.5	220
	240 h	223.4	-1.05	94.4	270.1
	432 h	344.7	-1.044	92.6	261
	720 h	229.8	-1.039	91.8	213.6
Copperized layer	24 h	195.5	-1.027	95.12	198.6
	72 h	143.8	-1.045	104.02	138.5
	240 h	194.8	-1.055	102.7	150.6
	432 h	218.9	-1.055	99.67	151.4
	720 h	212.6	-1.055	102.2	157.9

transfer process played a dominate role in the entire period. Meanwhile, the size of the loops decreased gradually with the extension of immersion time in an oscillatory manner. It is generally accepted [26] that the formation of corrosion product layer may cause a second time-constant in the Bode plot owing to the different structure, constitution and stress distribution between the corrosion product layer and metal. However, there was no distinct diversification in impedance modulus and phase angle plots of substrate and copperized layer which indicated that only one time-constant occurred during the entire period. Previous studies proved [27] that the resistance derived from porous thin corrosion products was so small which could not appear in impedance spectrum. Besides, the decrease of maximum phase angle and low-frequency deviation indicated that the deterioration of corrosion resistance was related to the attack by Cl⁻ or the permeation of dissolved oxygen.

In particular, the low-frequency impedance can accurately reflect the impedance variation of the samples, which was used to evaluate the corrosion resistance in general. Fig. 10 shows the variation of low-frequency impedances of substrate and the copperized layer. At initial stage, the value of low-frequency impedances increased because the formation of rust layer impeded the pitting corrosion of Cl⁻ and then decreased suddenly, which indicated that the rust layer was destroyed with high content of

Cl⁻ and oxygen diffusion corrosion was accelerated. After that, the value of low-frequency impedances declined gradually with the extension of immersion time (from 800 Ω to 400 Ω), suggesting that the existence of rust layer accelerated the progress of corrosion. However, the impedance of the coating was slightly higher than substrate.

The equivalent circuit is proposed in Fig. 11 to further analyze the electrochemical process of the electrode-electrolyte surface. In the fitted equivalent circuit, R_s corresponded to the solution resistance

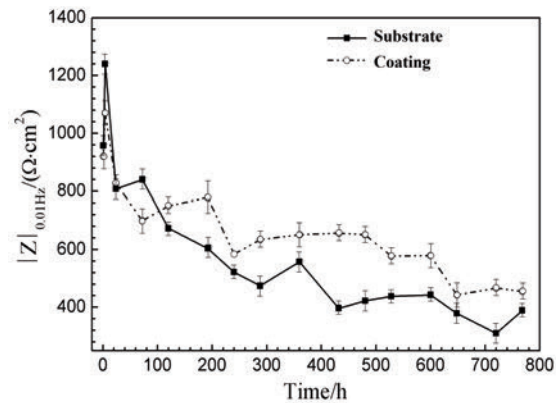


Figure 10. variation of low frequency modulus $|Z|_{0.01\text{Hz}}$ of Q235 steel and the copperized layer with immersion time

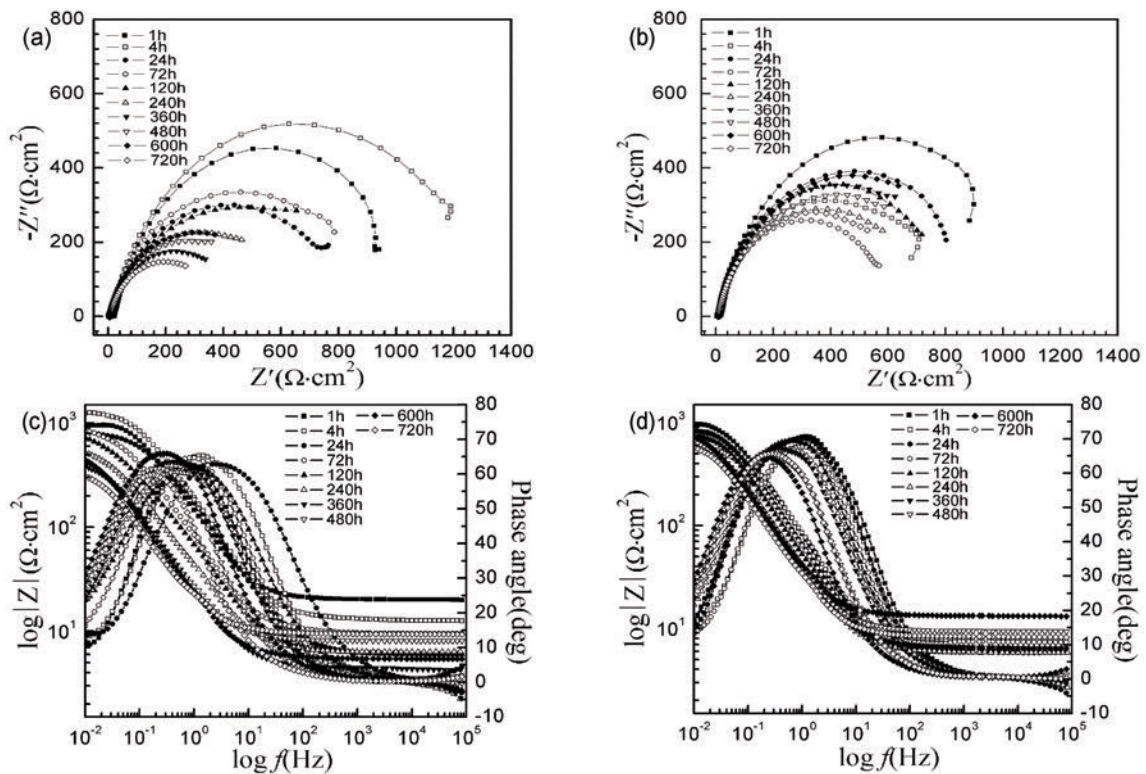


Figure 9. Nyquist plots and Bode plots of Q235 steel (a, c) and copperized layer (b, d) at different immersion time in 3.5 wt.% NaCl solution



from the reference electrode to the sample, R_{ct} was charge transfer resistance, and Q_c represented pseudo double layer capacitance.

Generally, the frequency response characteristics of the double layer capacitance on the metal electrode surface are not consistent with that of pure capacitor. For obtaining better agreement between the simulation and experimental data, the constant phase angle element (Q) is usually introduced to substitute pure capacitor, which is defined by Eq. (1) [28-30].

$$Q = Z_{CPE} = \frac{1}{Y_0} \cdot (j\omega)^{-n} \quad (1)$$

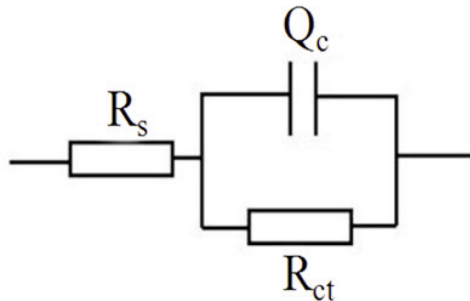


Figure 11. The equivalent circuit model used for fitting the impedance measurements of Q235 steel and the copperized layer immersed in 3.5 wt.% NaCl solution

where Y_0 is basic admittance ($\Omega^{-1} \cdot \text{cm}^{-2} \cdot \text{s}^{-n}$ or $\text{S} \cdot \text{cm}^{-2} \cdot \text{s}^{-n}$); n is frequency coefficient; j is imaginary unit ($j^2 = -1$); ω is angular frequency ($\omega = 2\pi f$, f is frequency).

The constant phase angle element depended on two important parameters which were frequency coefficient and basic admittance. The frequency coefficient was CPE exponent (between 0 and 1), which reflected the degree of interface deviation from the ideal capacitance. The basic admittance was the magnitude of admittance of CPE, which described the deviation physical quantity of the equivalent capacitance. The capacitance of the substrate was smaller than that of the coating at the primal phase (Fig. 12a and b) due to the roughness or heterogeneity of the sample surface. Some scholars suggested [31, 32] that the micro-roughness and surface heterogeneity might result in the alteration of capacitance, even the deviation of Nyquist. During the immersion process, the capacitances of substrate and the coating increased eventually approaching $5000 \mu\text{F} \cdot \text{cm}^{-2}$.

The corrosion products with porous structure were filled by water, so that it could not prevent the charge transfer and induced the increasing capacitance. Meanwhile, the trends of frequency coefficients of both electrodes were quite different, in which that of substrates fluctuated slightly and the coating decreased with time then tending towards stability.

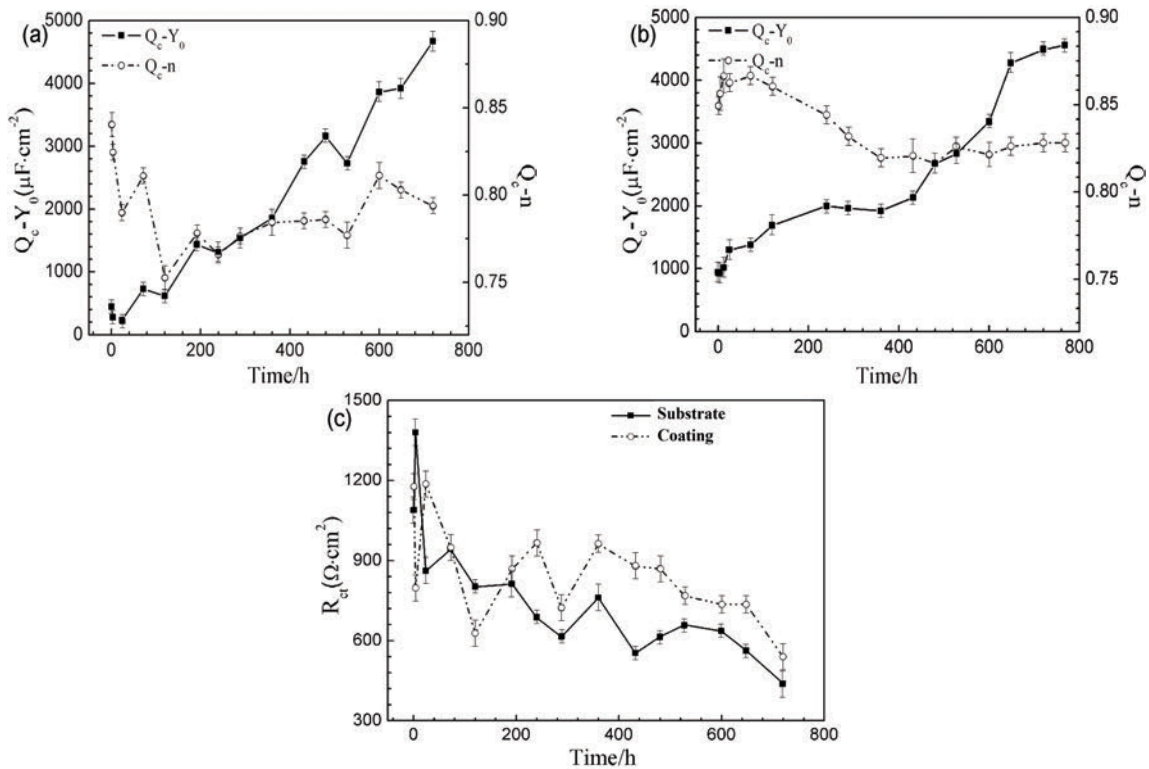


Figure 12. The variation of $Q_c \cdot Y_0$ and $Q_c \cdot n$ of Q235 steel (a) and the copperized layer (b) as well of the R_{ct} (c) with immersion time



Generally, the behavior of the double layer capacitance tended to pure capacitance. From the overall view, the frequency coefficient of the substrate fluctuated around 0.775 (Fig. 12a) during the corrosion process, which indicated the mass transfer and charge transfer simultaneously occurred. The decrease of frequency coefficient at initial stage can be explained by that the unstable rust layer and the contact between electrolyte and substrate led to the aggravation of anodic dissolution. With the extension of immersion time, the formation of rust layer was stabilized, and the frequency coefficient became more and more stable. As for the coating (Fig. 12b), the corrosion behavior at the early stage was close to pure capacitance, then the frequency coefficient decreased relatively due to the permeation of electrolyte and destruction of the coating. The corrosion behavior of coating was more and more similar to the substrate. In addition, the value of charge transfer resistance decreased relatively (Fig. 12c) with the extension of immersion time, which indicated that the presence of the rust layer reduced the corrosion resistance of substrate and copper layer.

3.4. Corrosion Mechanisms

In the process of immersion, yellow corrosion products covered the surface of substrate and the coating, which could be easily removed under slight disturbance. According to electrochemical measurements, the corrosion products could not enhance corrosion resistance of substrate and the coating.

Since the electrochemical reactions of carbon steel in sodium chloride solution have been widely explored [33-35], the typical anodic and cathodic reactions could be defined in accordance with the following equations:

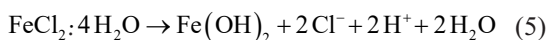
anodic:



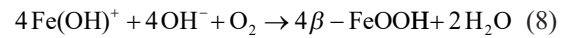
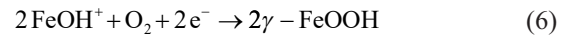
cathodic:



However, as mentioned above, the adsorption of Cl^- on the surface destabilized the electrochemical data before the stable corrosion product layer formed:



Subsequently, the formation of FeOOH film was stabilized after the Cl^- was separated from the sample surface:



Many scholars pointed that the phase transformations between $\beta/\gamma\text{-FeOOH}$ to $\alpha\text{-FeOOH}/\text{Fe}_3\text{O}_4$ thickened the rust layer, which enhanced the corrosion resistance of the sample. However, the formation of rust layer accelerated the corrosion in this paper. Hu pointed out [35] that the transformation of $\gamma\text{-FeOOH}$ was highly correlated with the nature of solution during the corrosion process, and suggested that the transformation of $\gamma\text{-FeOOH}$ to Fe_3O_4 occurred in acidulous sodium chloride solution (CO_2 dissolution). Stratmann and Hoffman [36] showed that the reduction from $\gamma\text{-FeOOH}$ to Fe_3O_4 occurred around the potential of -0.65 V. Based on above discussion, the corrosion potential of the substrate was -0.74 V during the immersion process, which indicated that the $\gamma\text{-FeOOH}$ (transformed from iron hydroxide) would undergo a reduction reaction continuously:

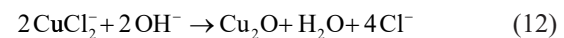


According to the results of the electrochemical measurements, the corrosion rate was still increasing even if the Fe_3O_4 was formed in later corrosion period, which attributed to the attack of Cl^- and more oxygen diffusion path. Thus, the corrosion resistance of substrate trended down consistently in 3.5 wt.% NaCl solution.

As for the copperized layer, the cathode reaction was consistent with substrate, but the anode reaction was:



Generally, the formation of cuprous oxide was accelerated when the concentration of insoluble CuCl_2^- was considerable high, and the reaction equilibrium constant could attained 10^{20} in 25°C :



However, the XRD and EDS results indicated that oxidation of the coating was slight and the constitution of corrosion products was mainly iron oxides. It can be deduced that although the copper content in sediment layer attained 80 at.%, the dissolved copper ions mainly existed in the electrolyte rather than forming insoluble substances. Thus, the



copper ions in electrolyte had a unique influence on the rust formation. Previous studies showed that [37] the copper enriched on the surface of rust layer can inhibit the formation of crystalline phases (such as α -FeOOH and γ -FeOOH) and promote the generation of amorphous phases. The solution of copper into FeOOH could damage the hydroxyl bonding and oxygen vacancy, which refined the crystalline structure. The existence of copper promoted the formation of amorphous phases, which converted the Fe(II) Hydroxo-complexes to amorphous δ -FeOOH. Meanwhile, the amorphous phases with few holes and cracks controlled the diffusion of oxygen, which restrained the oxidation-reduction reaction of the iron hydroxide at the bottom of the rust layer.

4. Conclusion

The fabrication of protective copperized layer on the surface of Q235 steel alloy via double glow plasma surface alloying technology was to improve the marine fouling organisms attach and multiply on the surface of marine structures. The copperized layer consisted of deposited layer and diffusion layer. During double glow treatment, the bombardment by Ar⁺ activated the surfaces of target and substrate. The copper atoms were sputtered from target to substrate and diffused into the surface under the high temperature device chamber environment. The adhesion between coating and substrate was strong because of the metallurgical bonding effects.

The evolution of the surface corrosion morphology indicated that the corrosion products of Q235 steel were mainly β -FeOOH, γ -FeOOH, and α -FeOOH in the early stage of corrosion process. The whisker-like structure of α -FeOOH grew on the surface of γ -FeOOH, then β -FeOOH transformed into γ -FeOOH to achieve thermodynamically equilibrium. The copper ions dissolved in the solution can restrain the transition of iron hydroxide and promote the formation of amorphous δ -FeOOH phase. The amorphous phase with few holes and cracks controlled the diffusion of oxygen, which restrained the oxidation-reduction reaction of the iron hydroxide at the bottom of the rust layer. Based on the electrochemical measurement, both coating and substrate presented similar electrochemical characteristics. However, the corrosion current density (I_{corr}) and charge transfer resistance (R_{ct}) of the coating presented a better corrosion resistance than Q235 steel.

Acknowledgements

This project was supported by the National Natural Science Foundation of China (No. 51874185) and A project funded by the Priority Academic

Program Development of Jiangsu Higher Education Institutions.

References

- [1] R. Jellali, I. Campistron, P. Pasetto, A. Laguerre, F. Gohier, C. Hellio, J.-F. Pilard, J.-L. Mouget, *Prog. Org. Coat.*, 76 (9) (2013) 1203-1214.
- [2] W. Wang, Z. Cao, *Sci. China-Technol. Sci.*, 59 (12) (2016) 1968-1970.
- [3] C. Li, M. Atlar, M. Haroutunian, C. Anderson, S. Turkmen, *Ocean Eng.*, 159 (2018) 481-495.
- [4] C.-F. Flach, C. Pal, C.J. Svensson, E. Kristiansson, M. Östman, J. Bengtsson-Palme, M. Tysklind, D.G. Joakim Larsson, *Sci. Total Environ.*, 590-591 (2017) 461-468.
- [5] S. Soroldoni, F. Abreu, Í. Braga Castro, F. Andrei Duarte, G. Lopes Leães Pinho, *J. Hazard. Mater.*, 330 (2017) 76-82.
- [6] X. Gao, J. Yang, Y. Zuo, Y. Tang, J. Xiong, *Corrosion Sci.*, 51 (2009) 1822-1827.
- [7] Z. Yang, W. Liang, Q. Miao, B. Chen, Z. Ding, N. Roy, *Mater. Res. Express.*, 5(4) (2018) 046408
- [8] S. Cui, Q. Miao, W. Liang, B. Li, *Appl. Surf. Sci.*, 428 (2018) 781-787.
- [9] D.B. Wei, H.X. Liang, S.Q. Li, F.K. Li, F. Ding, S.Y. Wang, Z.L. Liu, P.Z. Zhang, *J. Min. Metall. Sect. B-Metall.*, 55 (2) (2019) 227-234.
- [10] C. Xiaohu, Z. Pingze, W. Dongbo, D. Feng, L. Fengkun, W. Xiangfei, M. Shijian, *Mater. Lett.*, 215 (2018) 292-295.
- [11] S. Xu, P. Munroe, J. Xu, Z. Xie, *Surf. Coat. Technol.*, 307 (2016) 470-475.
- [12] D. Zhang, X. Gao, G. Su, L. Du, Z. Liu, J. Hu, *J. Mater. Eng. Perform.*, 26 (6) (2017) 2599-2607.
- [13] M. Bagherzadeh, H. Haddadi, M. Iranpour, *Prog. Org. Coat.*, 101 (2016) 149-160.
- [14] D. de la Fuente, I. Díaz, J. Alcántara, B. Chico, J. Simancas, Irene Llorente, J.A. Jimenez, P. Adeva, M. Morcillo, *Mater. Corros.*, 67 (3) (2016) 227-238.
- [15] J. Calero, J. Alcántara, B. Chico, I. Díaz, J. Simancas, D. de la Fuente, M. Morcillo, *Corros. Eng. Sci. Technol.*, 52 (3) (2017) 178-187.
- [16] H. Xiao, W. Ye, X. Song, Y. Ma, Y. Li, *Materials.*, 10(11) (2017) 1262.
- [17] D. de la Fuente, J. Alcántara, B. Chico, I. Díaz, J.A. Jiménez, M. Morcillo, *Corrosion Sci.*, 110 (2016) 253-264.
- [18] X.Q. Liu, Z. Liu, J.D. Hu, Z.G. Hou, Q. Tian, H.Z. Wang, *Anti-Corros. Methods Mater.*, 63 (4) (2016) 281-288.
- [19] Q. Xu, Ke. Gao, W. Lv, X. Pang, *Corrosion Sci.*, 102 (2016) 114-124.
- [20] H. Cano, I. Díaz, D. de la Fuente, B. Chico, M. Morcillo, *Mater. Corros.*, 69 (1) (2018) 8-19.
- [21] L. Huang, Z. Yin, N.G.A. Cooper, W. Yin, E. Tveden Bjerglund, B.W. Strobel, H.C.B. Hansen, *J. Hazard. Mater.*, 345 (2018) 18-26.
- [22] S. Ah Park, S.H. Kim, Y.H. Yoo, J.G. Kim, *Met. Mater.-Int.*, 21 (3) (2015) 470-478.
- [23] S. Kožuh, L. Vrsalović, M. Gojić, S. Gudić, B. Kosec, *J. Min. Metall. Sect. B-Metall.*, 52 (1) (2016) 53-61.



- [24] Q. Jiang, Q. Miao, F. Tong, Y. Xu, B. Ren, Z. Liu, Z. Yao, Acta., 115 (2014) 644-656.
- [25] H. Ezuber, A. Al Shater, Desalin. Water Treat., 57 (15) (2015) 6670-6679.
- [26] J. Wei, J. Dong, Y. Zhou, X. He, C. Wang, W. Ke, Mater. Charact., 139 (2018) 401-410.
- [27] S.Y. Lu, K.F. Yao, Y.B. Chen, M.H. Wang, N. Chen, X.Y. Ge, Corrosion Sci., 103 (2016) 95-104.
- [28] R.M. Souto, L. Fernández Mérida, S. González, D.J. Scantlebury, Corrosion Sci., 48 (5) (2006) 1182-1192.
- [29] D. Mareci, G. Bolat, R. Chelariu, D. Sutiman, C. Munteanu, Mater. Chem. Phys., 141 (1) (2013) 362-369.
- [30] G. Bolat, D. Mareci, S. Iacoban, N. Cimpoesu, C. Munteanu, J. Spectrosc., (2013) 714920.
- [31] P. Gümpel, A. Hoerthnagl, Mater. Corros., 67(6) (2016) 607-620.
- [32] C. José Felice, G. Alfredo Ruiz, C. Solitons Fractals., 84 (2016) 81-87.
- [33] J. Hu, S. Cao, J. Xie, Anti-Corros. Methods Mater., 60 (2) (2013) 100-105.
- [34] J.L. Xie, K.F. Jin, X.B. Jiang, J.D. Lu, J.Y. Hu, Surface Technology., 43 (2) (2014) 55-59.
- [35] J.Y. Hu, S.A. Cao, J.L. Xie, Acta Phys.-Chim. Sin., 28 (5) (2012) 1153-1162.
- [36] M. Stratmann, K. Hoffmann, Corrosion Sci., 29 (11) (1989) 1329-1352.
- [37] K. Seong Jong, J. Seok Ki, Trans. Nonferrous Met. Soc. China., 19 (s1) (2009) 50-55.

KOROZIVNO PONAŠANJE BAKARNOG PREMAZA NANETOG NA Q235 ČELIK TEHNIKOM PLAZME DVOSTRUKOG SJAJA

Z.-G. Yang ^{a,*}, W.-P. Liang ^{a,*}, Y.-L. Jia ^{b,c,*}, Q. Miao ^a, Z. Ding ^a, Y. Qi ^a

^a Fakultet za nauku o materijalima i tehnologijama materijala, Univerzitet za aeronautiku i astronautiku u Nandingu, Nanding, Kina

^b Fakultet za nauku o materijalima i inženjerstvo materijala, Centralnojužni univerzitet, Čangša, Kina

^c Fakultet za nauku o materijalima i tehnologijama materijala, Tehnološki univerzitet u Pekingu, Peking, Kina

Apstrakt

U ovom radu je predstavljen uticaj bakarnog sloja nanetog na površinu Q235 čelika tehnikom plazme dvostrukog sjaja za legiranje na naslage nepoželjnih organizama nastalih obrastanjem koji se nalaze na površini brodskih struktura. Skenirajući elektronski mikroskop (SEM) i XRD analiza su korišćeni za ispitivanje mikrostrukture i kompozicije faza premaza. Koroziono ponašanje podloge i premaza je ispitivano u 3,5 wt.% rastvoru NaCl. Rezultati su pokazali da je zaštitni premaz imao novu strukturu koja se sastojala od spoljnog sloja nastalog taloženjem (85 μm) i unutrašnjeg difuzionog sloja (51 μm), i koja je imala visok napon prijanjanja zbog uticaja metalurškog vezivanja. Koroziono ponašanje podloge i premaza je detaljno ispitano. Tokom početne faze korozije na Q235 čeliku su se uglavnom pojavili β-FeOOH, γ-FeOOH i α-FeOOH. Nakon početne faze α-FeOOH se formirao u obliku dlake na površini γ-FeOOH, a β-FeOOH je prešao u γ-FeOOH da bi se postigao termodinamički ekvilibrijum. Rastvoreni joni bakra u rastvoru su doprineli da se formiraju jedinstveni produkti korozije što je pokrenulo promenu gvožđe hidroksida i podstaklo formiranje amorfnih faza. Na osnovu elektrohemijskih merenja, premaz je imao nižu trenutnu korozivnu gustinu, a višu otpornost prenosa naboja od podloge. Otpornost na koroziju je bila veća kod bakarnog sloja nego kod Q235 čelika.

Ključne reči: Tehnika plazme duplog sjaja; Legiranje površine plazmom; Bakarni sloj; Sistem protiv obrastanja; Koroziono ponašanje; Sloj rde.



